Hindawi
Advances in Materials Science and Engineering
Volume 2018, Article ID 4829508, 6 pages
https://doi.org/10.1155/2018/4829508

Research Article

Effect of Power Cycling and Heat Aging on Reliability and IMC Growth of Sn-5Sb and Sn-10Sb Solder Joints

Tatsuya Kobayashi,[1] **Ikuo Shohji**,[1] **and Yusuke Nakata**[1,2]

[1]*Graduate School of Science and Technology, Gunma University, 1-5-1 Tenjin-cho, Kiryu 376-8515, Japan*
[2]*Calsonic Kansei, Co., Ltd., 7-1 Sakae-cho, Sano 327-0816, Japan*

Correspondence should be addressed to Tatsuya Kobayashi; t172b601@gunma-u.ac.jp

Received 26 December 2017; Revised 18 April 2018; Accepted 23 April 2018; Published 9 May 2018

Academic Editor: Abílio De Jesus

Power cycle reliability of solder joints with Sn-5Sb (mass%) and Sn-10Sb (mass%) alloys was investigated. The effects of power cycling and heat aging on the growth of intermetallic compound (IMC) layers at the interfaces between Sn-Sb alloys and Cu plates were also investigated. In the power cycling test, the solder joint with Sn-10Sb has high reliability compared with that of Sn-5Sb. IMC layers grew in both joints with increasing number of power cycles. Compared with Sn-5Sb and Sn-10Sb, difference in growth kinetics of IMC layers was negligible. A similar tendency was observed in the heat aging test. Compared with the power cycling and the heat aging, growth of IMC layers at the aging temperature of 200°C is faster than that in the power cycling test at the temperature range of 100°C to 200°C, while that at the aging temperature of 100°C, the growth is slower. On the basis of the comparison between the power cycling and the heat aging, it was clarified that growth kinetics of IMC layers in the power cycling can be predicted by investigating growth kinetics of the IMC layer at the temperatures in the vicinity of the peak temperature in power cycling.

1. Introduction

Sn-Pb alloys have been used for the electronic products as a joint material for a long time. However, due to environmental considerations, the use of Pb is restricted, and Pb-free solder is required [1–6]. Although many researchers have developed the substitutes for the eutectic Sn-Pb solder, there has been little study concerning the high-temperature Sn-Pb solder [7]. The high-temperature solder is applied to the power semiconductor modules as a die bonding material. For the application of such Pb-free solder, both high thermal fatigue reliability and high heat resistance are required.

An Sn-Sb alloy is one of the potential substitute materials for the high-temperature Sn-Pb solder [7–12]. It has been reported that Sn-5Sb (mass%) has excellent thermal fatigue behaviors and relatively high fracture strength [13, 14]. Furthermore, the Sn-5Sb alloy has been standardized by Japanese Industrial Standards (JIS) Z 3282 and International Organization for Standardization (ISO) 9453. In addition, in Sn-Sb alloys with high concentration of Sb, mechanical strength is improved by solid solution of Sb in the β-Sn matrix and dispersion of Sb-Sn compounds. Therefore, Sn-10Sb (mass%) with a higher amount of Sb was chosen as another candidate together with Sn-5Sb. Sn-5Sb and Sn-10Sb are hypoperitectic and approximately peritectic system alloys, respectively. Mechanical, melting, and electrical properties of these solders have been investigated [1, 15, 16]. However, there are not many reports about the heat cycle test using solder joints. Furthermore, the difference between growth kinetics of the intermetallic compound (IMC) layer during power cycling and that during heat aging has not been clarified yet.

The aim of this study is to investigate the reliability of solder joints with Sn-5Sb and Sn-10Sb alloys in the power cycle. Moreover, the effect of the number of power cycles and heat aging time on IMC growth in those solder joints was investigated.

2. Experimental Procedure

2.1. Specimen Preparation. Solder foils of Sn-5Sb and Sn-10Sb alloys were prepared. Table 1 shows melting properties

Table 1: Melting properties of solder investigated.

Chemical compositions (mass%)	Solidus temperature (°C)	Melting finish temperature (°C)
Sn-5Sb	240	248
Sn-10Sb	248	254

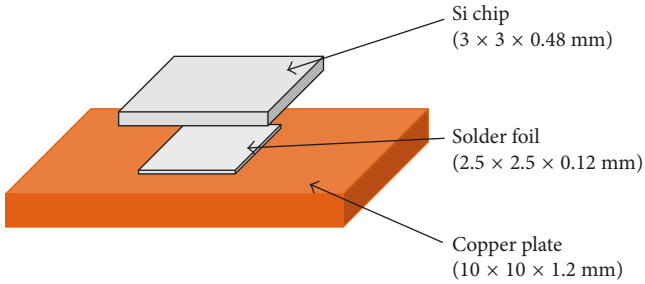

Figure 1: Shape and dimensions of the specimen for the power cycling test and heat aging test.

of those solders investigated using differential scanning calorimetry (DSC) at a heating rate of 10°C/min. Figure 1 shows the shape and the size of the solder joint specimen. A Ti/Ni/Au layer was formed on the surface of a Si-chip. The thickness of the Ti/Ni/Au layers was 100/100/100 nm, respectively. The surface of the Cu plate was polished with a #800 polishing paper. A flux (Senju Metal Industry: Deltalux 529D-1) was applied onto the Cu plate and a solder foil is placed on the flux, and then the Si-chip is placed on the top of the solder foil. Reflow soldering was conducted at a temperature that is 30°C higher than the melting finish temperature with an infrared image furnace in a vacuum of approximately 5 Pa. In reflow soldering, the joint was loaded at 0.02 N.

After bonding, specimens were cleaned with methyl alcohol. In this study, bonded specimens were used for the power cycling test and the heat aging test.

2.2. Microstructural Observation. To observe the microstructures of the joints, they were embedded in epoxy resin and cross sections perpendicular to the longitudinal direction were cut out. Afterwards, the cross sections were polished with #500–#4000 polishing papers and were subsequently polished using 1 μm alumina powder suspension. After polishing, microstructural observation was conducted using a laser microscope and an electron probe X-ray microanalyzer (EPMA).

2.3. Power Cycling Test. The power cycling test was conducted using a power cycle test machine. Figure 2 shows the temperature profile in the power cycling test. In this study, the power cycling test conditions were based on Japan Electronics and Information Technology Industries Association (JEITA) standards (no. ED-4701-602). The profile is 100°C to 200°C with a cycle time of 20 sec, a heating time of 2 sec, and cooling time of 18 sec. The test was performed for 1000, 5000, and 10000 cycles. Converted into process time in the test, they are 20000 sec (5.6 h), 100000 sec (27.8 h), and

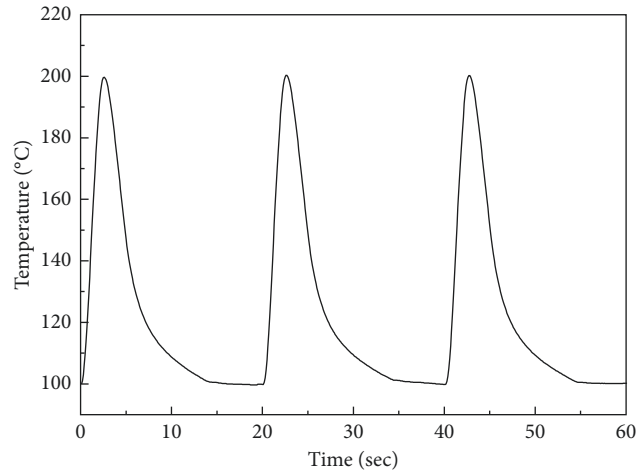

Figure 2: Temperature profile in the power cycling test.

200000 sec (55.6 h), respectively. After the test, the crack in the solder joint was observed using a scanning acoustic tomograph (SAT). In addition, the cross sections of the solder joints were observed using an EPMA. Moreover, the thickness of the IMC layers was measured at 10 points at an interval of 10 μm in the cross-sectional image.

2.4. Heat Aging Test. The heat aging test was conducted using a furnace. The test was conducted with isothermal aging at 100°C and 200°C for 5.6, 27.8, and 55.6 hours that are equivalent to the test time in 1000, 5000, and 10000 cycles for the power cycling test. After the test, microstructural observation for the cross section of the joint was conducted using the EPMA. Moreover, the thickness of the IMC layers was measured at 10 points at an interval of 10 μm in the cross-sectional image.

3. Results and Discussion

3.1. Microstructures of Joints. Figure 3 shows an optical image and a back-scattered electron image of the cross section of the joint with Sn-5Sb and the EPMA analysis result for it. From the EPMA mapping analysis result, Sn and Cu were detected in the IMC formed in the joint of Cu/Sn-5Sb.

Figure 4 shows an optical image and a back-scattered electron image of the cross section of the joint with Sn-10Sb and the EPMA analysis result for it. From the EPMA mapping analysis result, Sn-Cu was also detected in the IMC layer and Sb-Sn was confirmed in the joint with Sn-10Sb. Figure 5 shows the Sn-Sb binary phase diagram [17]. From the diagram, it is found that investigated Sn-Sb alloys consist of β-Sn and Sb-Sn phases. Moreover, it has been reported that the distribution of Sb-Sn particles was observed in Sn-

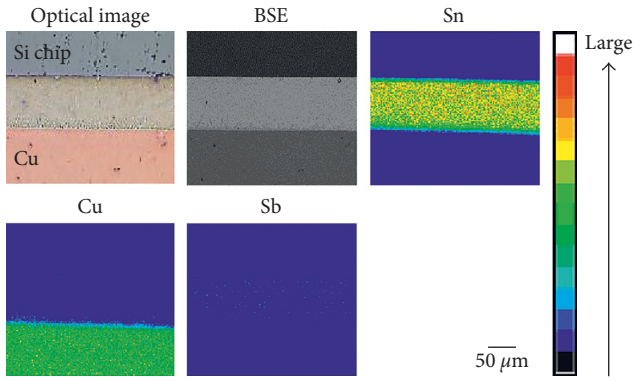

Figure 3: Optical image and back-scattered electron image of cross section of the solder joint with Sn-5Sb and its EPMA mapping analysis result.

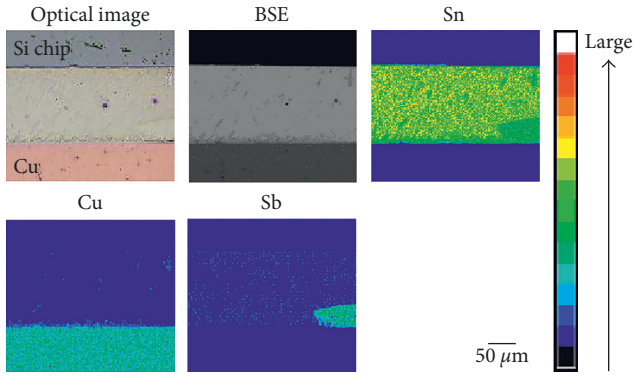

Figure 4: Optical image and back-scattered electron image of cross section of the solder joint with Sn-10Sb and its EPMA mapping analysis result.

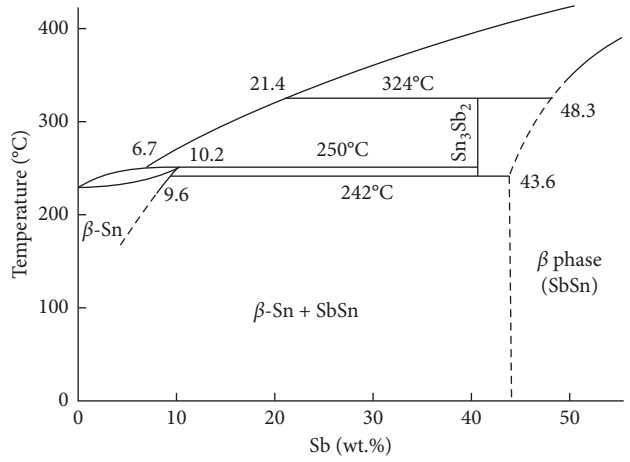

Figure 5: Sn-Sb binary phase diagram [17].

10Sb [15]. Therefore, Sb-Sn particles were also formed in the joint with Sn-10Sb in this study.

3.2. Power Cycling Test. Figure 6 shows SAT images of Sn-Sb solder joints for 0, 1000, 5000, and 10000 cycles in the power

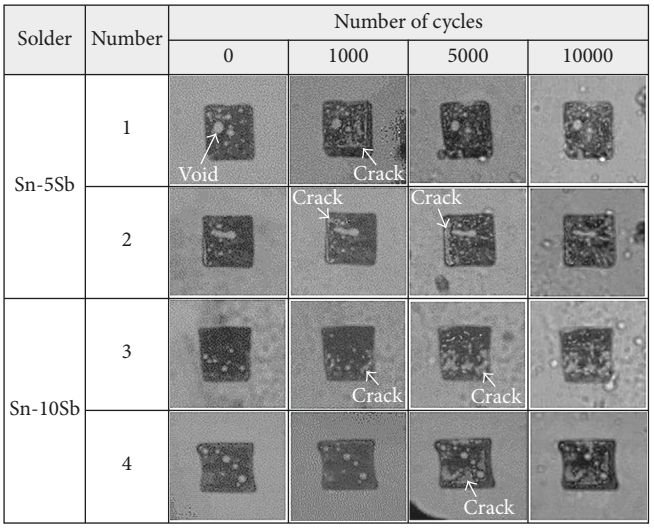

Figure 6: Scanning acoustic tomography images of solder joints after the power cycling test.

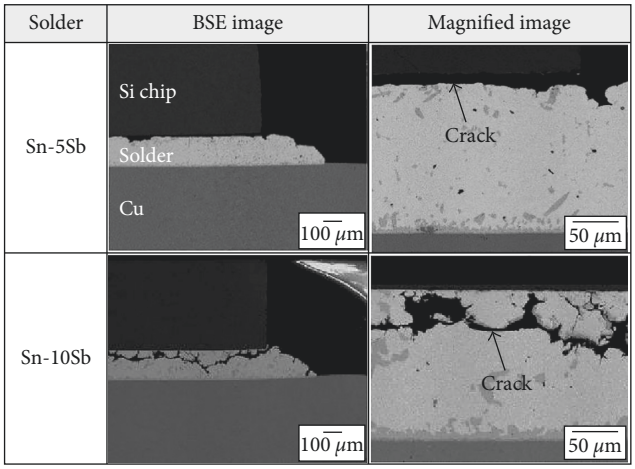

Figure 7: Back-scattered electron images of cross sections of solder joints after the power cycling test.

cycling test. In the images, while the crack in the solder joint with Sn-5Sb was remarkable at 1000 cycles, the crack was notably observed at 5000 cycles in the joint with Sn-10Sb. Hence, it was confirmed that the solder joint with Sn-10Sb has high reliability compared with that with Sn-5Sb. Figure 7 shows back-scattered electron images of cross sections of solder joints after the power cycling test. Although the crack formed and progressed at the interface between the solder and the Si-chip in the joint with Sn-5Sb, the crack progressed in the solder forming a zigzag pattern in the joint with Sn-10Sb. In Sn-5Sb, there is a large difference between coefficient of thermal expansion (CTE) of the Sn-Sb alloy and that of the Si so that the crack is easily formed and it grew at the joint interface between the solder and the Si chip. In Sn-10Sb, with an increase of the Sb content, the CTE of the Sn-Sb alloy decreases and is close to that of Si, and thus the crack easily grows in the solder joint. Furthermore, coarse Sb-Sn compounds in the Sn-Sb alloy are effective to prevent the crack growth.

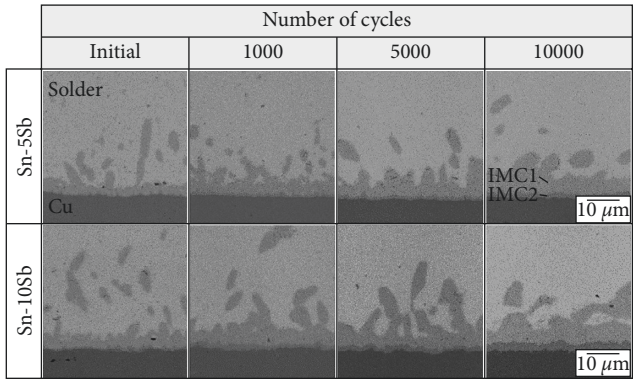

FIGURE 8: Back-scattered electron images of cross sections of IMC layers formed in interfaces of Sn-Sb/Cu joints after the power cycling test.

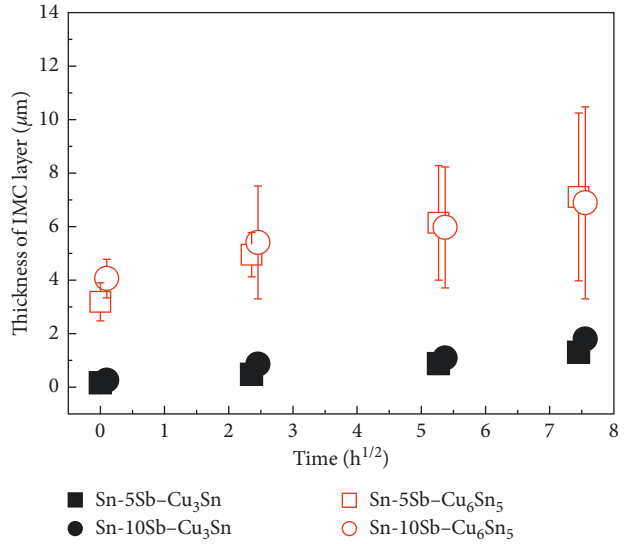

FIGURE 9: Thickness of IMC layers versus square root of the power cycling time.

Figure 8 shows back-scattered electron images of IMC layers formed in the interfaces of the Sn-Sb/Cu joints after the power cycling test. In the images, two IMC layers were observed in the Sn-Sb/Cu joints. From the quantitative analysis results, the dark-gray layer and the bright-gray layer were inferred to be Cu_3Sn and Cu_6Sn_5, respectively. These IMC layers tend to increase with the increasing number of power cycles. Figure 9 shows the relationship between the thickness of IMC layers and processing time of the power cycling test. The thickness of IMC layers in the joints with both alloys increased with increasing the processing time. Compared with Sn-5Sb and Sn-10Sb, the difference in growth kinetics of IMC layers is negligible.

3.3. Heat Aging Test. Figures 10 and 11 show back-scattered electron images of cross sections of Sn-Sb solder joints after the heat aging test at 100°C and 200°C, respectively. In the images, two IMC layers were observed in Sn-Sb/Cu joints, regardless of aging temperature. The dark-gray layer and the

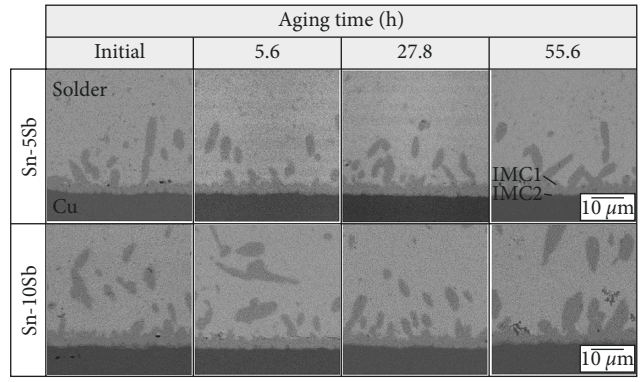

FIGURE 10: Back-scattered electron images of cross sections of IMC layers formed in interfaces of Sn-Sb/Cu joints after heat aging test at 100°C.

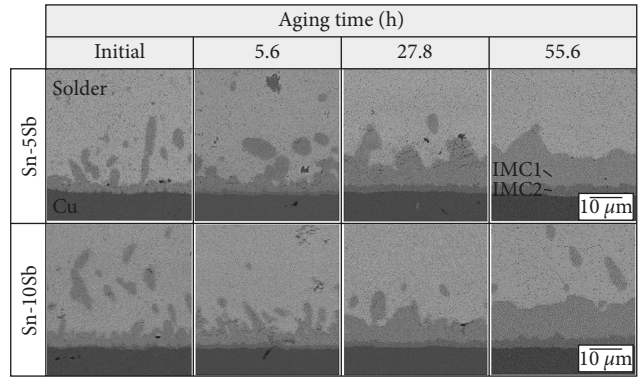

FIGURE 11: Back-scattered electron images of cross sections of IMC layers formed in interfaces of Sn-Sb/Cu joints after heat aging test at 200°C.

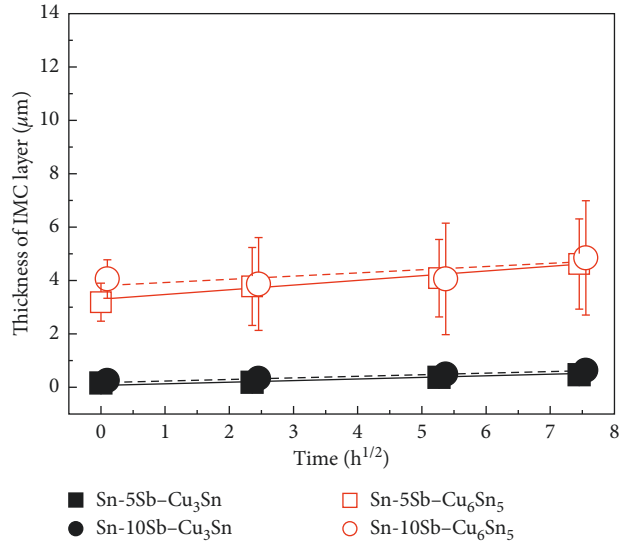

FIGURE 12: Thickness of IMC layers versus square root of heat aging time at 100°C.

bright-gray layer were inferred to be Cu_3Sn and Cu_6Sn_5, respectively, as well as the joint after the power cycling test. Figures 12 and 13 show the relationship between the

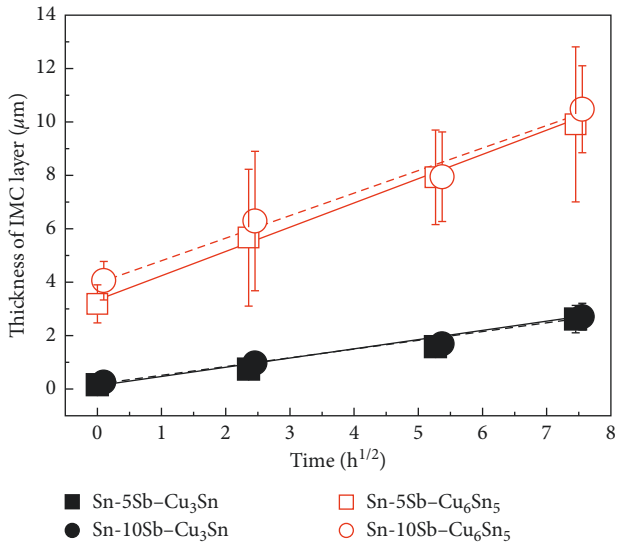

Figure 13: Thickness of IMC layers versus square root of heat aging time at 200°C.

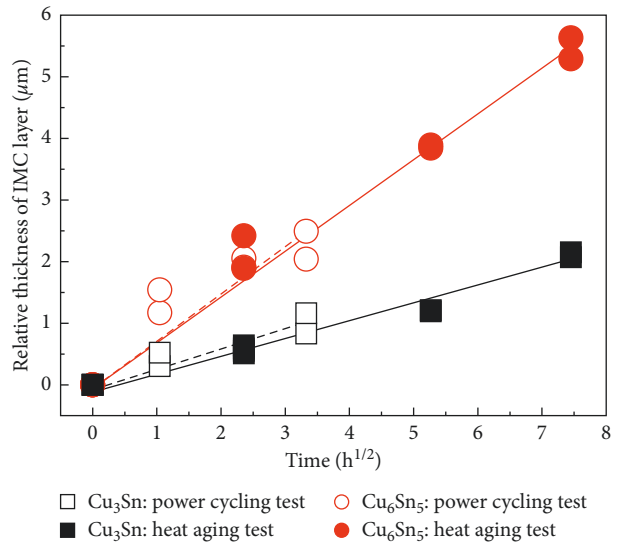

Figure 14: Relationship between the relative thickness of IMC layers in Sn-Sb/Cu joints and one-fifth of an actual processing time in the power cycling test, and relationship between those and aging time in the aging test at 200°C.

thickness of IMC layers and the heat aging time at 100°C and 200°C, respectively. The thickness of IMC layers in both joints increased with increasing heat aging time and aging temperature. In general, when the thickness of the IMC layer is plotted against the square root of heat aging time under constant temperature, the relationship obeys the following equation [18]:

$$X = \sqrt{Kt} + X_0, \quad (1)$$

where X is the thickness of IMC layer, K is the interdiffusion coefficient, t is the heat aging time, and X_0 is the thickness of the IMC layer in the as-soldered state.

Compared with Sn-5Sb and Sn-10Sb, the difference in growth kinetics of IMC layers in both the joints is negligible. Compared with the results of the power cycling test as shown in Figure 9, IMC layers aged at 200°C are thicker than those in power cycling under the same processing time, while those aged at 100°C are thinner.

Figure 14 shows the relationship between the average thickness of IMC layers in Sn-Sb/Cu joints and one-fifth of an actual processing time of the power cycling test. That time is equivalent to the time when the joint is exposed at the temperature over 160°C. The relationship between the average thickness of IMC layers in the joints and the heat aging time at 200°C is also shown in the figure. Now, the thickness of IMC layers in the figure was obtained by subtracting that investigated by aging at 100°C (as shown in Figure 12) from each data. From the figure, it was found that the growth kinetics of IMC layers in power cycling corresponds well with that in aging at 200°C when the processing time in power cycling is defined to be the time when the joint is exposed at the temperature over 160°C. This means that the growth kinetics of IMC layers in power cycling can be predicted by investigating the growth kinetics of the IMC layer at the temperatures in the vicinity of the peak temperature in power cycling.

4. Summary

In this study, power cycle reliability of the solder joints with Sn-5Sb (mass%) and Sn-10Sb (mass%) and the effects of processing time in the power cycling test and heat aging time on growth kinetics of IMC layers formed at the Sn-Sb/Cu interfaces were observed. The obtained results are summarized as follows.

(1) In the power cycling test, the solder joint with Sn-10Sb has high reliability compared with Sn-5Sb. In both Sn-Sb/Cu joints, two Cu-Sn IMC layers were observed, and those were inferred to be Cu_3Sn and Cu_6Sn_5. The thickness of IMC layers in both joints increased with increasing the processing time. The difference in growth kinetics of IMC layers in both joints is negligible.

(2) In the heat aging test, the similar IMC layers were formed at the joint interfaces in both Sn-Sb/Cu joints. For growth kinetics of the layers, the tendency similar to that in the power cycling test was observed.

(3) Comparing heat aging at 100°C and 200°C with power cycling in the temperature range from 100°C to 200°C, it was found that growth kinetics of IMC layers in power cycling corresponds well with that in aging at 200°C when the processing time in power cycling is defined to be the time when the joint is exposed at the temperature over 160°C. The result means that the growth kinetics of IMC layers in power cycling can be predicted by investigating the growth kinetics of the IMC layer at the temperatures in the vicinity of the peak temperature in power cycling.

Conflicts of Interest

The authors declare that they have no conflicts of interest.

References

[1] A. A. El-Daly, Y. Swilem, and A. E. Hammad, "Creep properties of Sn–Sb based lead-free solder alloys," *Journal of Alloys and Compounds*, vol. 471, no. 1-2, pp. 98–104, 2009.

[2] V. Chidambaram, J. Hattel, and J. Hald, "High-temperature lead-free solder alternatives," *Microelectronic Engineering*, vol. 88, no. 6, pp. 981–989, 2011.

[3] J. H. L. Pang, T. H. Low, B. S. Xiong, X. Luhua, and C. C. Neo, "Thermal cycling aging effects on Sn-Ag-Cu solder joint microstructure, IMC and strength," *Thin Solid Films*, vol. 462-463, pp. 370–375, 2004.

[4] S. Ahat, M. Sheng, and L. Luo, "Microstructure and shear strength evolution of SnAg/Cu surface mount solder joint during aging," *Journal of Electronic Materials*, vol. 30, no. 10, pp. 1317–1322, 2001.

[5] C. Lee, C. Y. Lin, and Y. W. Yen, "The 260°C phase equilibria of the Sn-Sb-Cu ternary system and interfacial reactions at the Sn-Sb/Cu joints," *Intermetallics*, vol. 15, no. 8, pp. 1027–1037, 2007.

[6] Y. Plevachuk, W. Hoyer, I. Kaban, M. Köhler, and R. Novakovic, "Experimental study of density, surface tension, and contact angle of Sn–Sb-based alloys for high temperature soldering," *Journal of Materials Science*, vol. 45, no. 8, pp. 2051–2056, 2010.

[7] Y. T. Chen and C. C. Chen, "Interfacial reactions in Sn–Sb/Ni couples," *Journal of the Taiwan Institute of Chemical Engineers*, vol. 43, no. 2, pp. 295–300, 2012.

[8] S. W. Chen, A. R. Zi, P. Y. Chen, H. J. Wu, Y. K. Chen, and C. H. Wang, "Interfacial reactions in the Sn–Sb/Ag and Sn–Sb/Cu couples," *Materials Chemistry and Physics*, vol. 111, no. 1, pp. 17–19, 2008.

[9] C. Lin, C. Lee, X. Liu, and Y. Yen, "Phase equilibria of the Sn-Sb-Ag ternary system and interfacial reactions at the Sn-Sb/Ag joints at 400°C and 150°C," *Intermetallics*, vol. 16, no. 2, pp. 230–238, 2008.

[10] S. W. Chen, C. C. Chen, W. Gierlotka, A. R. Zi, P. Y. Chen, and H. J. Wu, "Phase equilibria of the Sn-Sb binary system," *Journal of Electronic Materials*, vol. 37, no. 7, pp. 992–1002, 2008.

[11] M. Dias, T. Costa, O. Rocha, J. E. Spinelli, N. Cheung, and A. Garcia, "Interconnection of thermal parameters, microstructure and mechanical properties in directionally solidified Sn–Sb lead-free solder alloys," *Materials Characterization*, vol. 106, pp. 52–61, 2015.

[12] S. F. Corbin, "High-temperature variable melting point Sn-Sb lead-free solder pastes using transient liquid-phase powder processing," *Journal of Electronic Materials*, vol. 34, no. 7, pp. 1016–1025, 2005.

[13] K. Kobayashi, I. Shohji, and H. Hokazono, "Tensile and fatigue properties of miniature size specimens of Sn-5Sb lead free solder," *Materials Science Forum*, vol. 879, pp. 2377–2382, 2016.

[14] K. Kobayashi, I. Shohji, S. Koyama, and H. Hokazono, "Fracture behaviors of miniature size specimens of Sn-5Sb lead-free solder under tensile and fatigue conditions," *Procedia Engineering*, vol. 184, pp. 238–245, 2017.

[15] J. H. Kim, S. W. Jeong, and H. M. Lee, "Thermodynamics-aided alloy design and evaluation of Pb-free solders for high-temperature applications," *Materials Transactions*, vol. 43, no. 8, pp. 1873–1878, 2002.

[16] A. A. El-Daly, A. Fawzy, A. Z. Mohamad, and A. M. El-Taher, "Microstructural evolution and tensile properties of Sn–5Sb solder alloy containing small amount of Ag and Cu," *Journal of Alloys and Compounds*, vol. 509, no. 13, pp. 4574–4582, 2011.

[17] T. B. Massalski, *Binary Alloy Phase Diagrams*, ASM International, New York, NY, USA, 1990.

[18] K. H. Prakash and T. Sritharan, "Effects of solid-state annealing on the interfacial intermetallics between tin-lead solders and copper," *Journal of Electronic Materials*, vol. 32, no. 9, pp. 939–947, 2003.